Efficient scattering model of multi-layer systems with anisotropic films

JORDAN R. GILL,[1] ELENI PERIVOLARI, [2] MALGOSIA KACZMAREK,[2] AND GIAMPAOLO D'ALESSANDRO[1,*]

[1] *School of Mathematical Sciences, University of Southampton, Southampton SO17 1BJ, UK*
[2] *School of Physics & Astronomy, University of Southampton, Southampton SO17 1BJ, UK*
[*] *dales@soton.ac.uk*

Abstract: We present an intuitive and efficient method for modeling light propagation in layered isotropic and anisotropic media, the Iterated Ray Method. Considering a single layer sandwiched between semi-infinite layers, the infinite reflected and transmitted rays are summed to obtain effective Fresnel coefficients for the center layer. Thus, the system can be represented as two semi-infinite layers with an effective boundary. The model is coupled to a recursive algorithm to describe an arbitrarily large, layered system in the same way. It is numerically stable in the presence of evanescent waves and computationally efficient, both in terms of operation counts and vectorization. We demonstrate its importance for the optical analysis and optimization of layered media, such as those used in photo-addressable liquid crystal cells, thin film coatings, and Bragg gratings, by measuring the refractive index and thickness of a thin, azo-benzene dye, photo-alignment layer, PAAD-22E, on an ITO coated glass slide.

1. Introduction

Studying the behavior of light waves in layered media is essential to the understanding and design of elements such as anti-reflection coatings [1–3] and dielectric mirrors [4,5], or in any optical device that necessitates the use of multiple materials and layers, ranging from Bragg gratings [6,7] to Surface Plasmon Polaritons [8]. It is also vital for several techniques and devices. For example, ellipsometry [9] relies on the combination of experimental data and an understanding of the reflection properties of an arbitrary sample to determine the unknown refractive indices. The fitting of the experimental data can be complex if the layer is anisotropic and combined with additional materials [10]. Furthermore, organic photovoltaic cells, photo-aligned liquid crystal systems, or those with active command layers, increasingly comprise of a combination of different layers, including anisotropic materials. Understanding and modeling light propagation through such multi-layer geometries requires efficient and comprehensive algorithms.

There have been many studies of light propagation in stratified media, even in the more restricted field of birefrigent media [11–15] that is considered here. The book by Orfanidis [16] is an excellent introduction and review of the subject. Here we summarize the features of the two most common classes of methods.

The first and most common method for modeling wave propagation through multiple layers is known as the transfer matrix, or T-matrix, approach [17,18]. This method follows intuitively from applying the usual electromagnetic boundary conditions at each interface and accounting for the phase change of the fields in each layer to form a set of simultaneous equations. The equations are written in matrix form, with the result that the electric field on one side of the system is written in terms of the electric field on the other, i.e., the transmitted field is written as a linear combination of the incident and reflected fields.

It is well known, however, that this method suffers from problems of numerical instability in the presence of evanescent waves [19]. This instability arises as a result of the exponential terms in the model that account for the phase change of the fields across a layer. The backward

waves have a phase shift of $\exp(-iqL)$, where q is the normal part of the wave vector and L the thickness of the layer. These terms become exponentially increasing when the waves in the layer are evanescent (and q is imaginary) and the wave is "back-propagated" to the next layer. Conversely, the forward waves are exponentially decreasing, and the backward waves dominate numerically, resulting in the information about the forward wave being lost. There is also the issue that any numerical errors are grown exponentially by the backwards wave when propagating across a layer [20].

The scatting matrix, or S-matrix, is an alternative method that, while more complicated to implement, offers accurate solutions even when evanescent waves are present [19]. This is achieved by rewriting the T-matrix equations so that the outgoing waves are expressed in terms of the incoming ones. In the resulting matrix equations the forward and backward modes are separated and the numerical instability issues are avoided. The S-matrix is thus regarded as the leading standard in dealing with multi-layer propagation problems.

In this paper we present a method, which we call the Iterated Ray Method, that builds on a different tradition of beam propagation algorithms. These are based on summing reflected and transmitted waves, often referred to as Bremmer series [21]. Normally, the summation of a Bremmer series is performed numerically up to the required precision. However, in the case of the Iterated Ray Method the infinite sum is performed analytically, leading to a relatively simple set of exact equations. The method is based on a common textbook example (e.g. [22]) for studying three layer Fabry-Perot resonator systems. By considering the scattered light rays of the system, the total transmitted and reflected fields are found by summing all of the transmitted or reflected rays in a geometric series, allowing the system to be modeled as two layers with an effective transmission and reflection coefficient between them. The Iterated Ray Method extends this concept to systems with more than three layers. The final three layers of the system can iteratively be collapsed into two layers until an N layer system is also represented as 2 layer system with effective coefficients. The method is causal, namely, it follows the rays forward in time and never "back-propagates" any backward waves. This means that in the presence of evanescent waves there are only ever exponentially decaying terms appearing, and the Iterated Ray Method possesses all of the accuracy and stability of the S-matrix formulation. In fact, it can be shown formally that a Bremmer series is equivalent to the S-matrix method [23].

In the case of layered isotropic media, the reflection coefficient formula provided by the Iterated Ray Method matches exactly with previously reported results [16] obtained by algebraic manipulation of the T-matrix equations. In this paper, however, the corresponding transmission coefficient results (not given in [16]) are also presented. Furthermore, we also demonstrate how the Iterated Ray methodology is intuitively extendable to any system with multiple mixed modes, requiring only a knowledge of the reflection and transmission coefficients between the modes at each interface. As an example of this, we derive analytically the effective transmission and reflection coefficients of a single uniaxial layer with arbitrary optical axis between isotropic media (a Matlab code to implement the algorithm is available from Code 1, [24]).

In the next section we discuss the simplest implementation of the iterated ray method, the propagation through layered isotropic media. In section 4 we outline the steps required to calculate the reflection and transmission from a single anisotropic layer, with the full details of the calculations given in the Supplemental document. The calculations required for multiple anisotropic layers are sketched in section 5. We validate the code against other numerical simulations in section 6 and discuss its computational efficiency in section 7. In section 8, as a test of its applicability and speed, we analyze the experimental data of polarized light transmission through a system of a thin, azobenzene layer on a substrate. The conclusions summarize the main results of the paper and outline areas of future work.

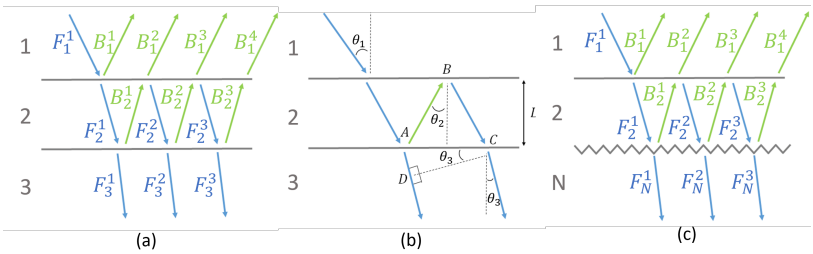

Fig. 1. Principle of the ray method. (a) In a three layer system, the input field in layer 1, F_1^1 is partially transmitted into medium 2 with amplitude F_2^1 and reflected back into layer 1 with amplitude B_1^1. At the interface between layers 2 and 3, F_2^1 is partially transmitted with amplitude F_3^1 and reflected back into layer 2 with amplitude B_2^1, and so on. (b) Calculation of the optical path length difference between two subsequent transmitted or reflected rays. (c) Recursive process to compute the effective reflection and transmission coefficients by representing the N layer system as a three layer system. The layers 3 to $N-1$ are replaced with an effective boundary, represented by a jagged interface.

2. Transmission and reflection of isotropic layered media

We introduce the iterated ray method by first considering layered structures of isotropic materials, formed of N layers each with refractive index n_j, $j = 1, 2, \ldots, N$. The first and last layers are both semi-infinite, as in figure 1(a), which depicts an $N = 3$ layer system. We assume that a plane wave with amplitude F_1^1 and vacuum wave number k_0 is propagating in the first layer, and that it is incident upon the structure at an angle θ_1 from the layer normal, as in figure 1(b). We study the waves propagation through the structure by considering the reflection and transmission of any rays incident upon a boundary. Starting with only the incident ray, an infinite number of forward and backward rays arise in each layer, the sum of which describe the total forwards and backwards fields in each layer. Our aim is to find a simple expression for their amplitudes. In particular, we are interested in finding the total field reflected back into layer 1 and the total transmitted field into layer N as a function of the incident field, allowing us to compute effective Fresnel coefficients for the layered structure. We first analyze this problem for a simple three layer structure, and then introduce in section 3 the recursion procedure that allows to compute the effective Fresnel coefficients for an arbitrary number of layers.

2.1. A single isotropic layer

We begin the outline of the iterated ray method by considering a system of three layers. The layers 1 and 3 are semi-infinite and sandwich layer 2, of finite thickness; see figure 1(a). The input field, F_1^1, is incident upon layer 2 in the forward direction, where one part of the field is reflected and the other part is transmitted into layer 2. Similarly, the transmitted field is split into reflected and transmitted fields at the interface between layer 2 and 3. In fact, every ray that is incident on an interface is split into two, with each of these split beams also being split each time they encounter an interface. This results in infinitely many rays arising in each layer, as depicted in figure 1(a). By summing all of the rays in each layer that are in the same direction, we can describe each layer i as having a single forwards and backwards field F_i and B_i, respectively.

The Fresnel coefficients can be used to describe the various rays in the system and calculate the total fields. From figure 1(a), we can see that the n'th ray to propagate into layer 3 is given by

$$F_3^n = t_{12}t_{23}e^{i\frac{\delta}{2}}\left(r_{23}r_{21}e^{i\delta}\right)^{n-1}F_1^1, \tag{1}$$

where t_{ij} and r_{ij} are the Fresnel transmission and reflection coefficients at the interface between layer i and layer j, respectively. Similarly, the n'th backward ray in layer 1 is given by

$$B_1^n = \begin{cases} r_{12}F_1 & n = 1 \\ t_{12}r_{23}t_{21}e^{i\delta}\left(r_{21}r_{23}e^{i\delta}\right)^{n-2}F_1 & n > 1. \end{cases} \tag{2}$$

The quantity δ is the phase difference between two subsequent rays. It is given by, see figure 1(b),

$$\begin{aligned} \delta &= k_0\left[\left(\left|\overrightarrow{AB}\right| + \left|\overrightarrow{BC}\right|\right)n_2 - \left|\overrightarrow{AD}\right|n_3\right] \\ &= k_0\left[2L\sec(\theta_2)n_2 - 2L\tan(\theta_2)\sin(\theta_3)n_3\right], \end{aligned} \tag{3}$$

where L is the thickness of layer 2. Applying Snell's Law then gives

$$\delta = 2k_0Ln_2\cos(\theta_2) = 2q_2L, \tag{4}$$

where $q_j = k_0n_j\cos(\theta_j)$. We can see from equation (4) that the phase change is just the normal component of the wave vector (q_j) multiplied by the layer thickness, as expected from standard wave propagation theory.

The sum of all of the transmitted and reflected rays can be reduced to a geometric series, which we can sum to obtain the effective transmission coefficients of the system as

$$F_3 = t_{13}F_1, \quad t_{13} = \frac{t_{12}t_{23}e^{i\frac{\delta}{2}}}{1 - r_{23}r_{21}e^{i\delta}}, \tag{5a}$$

$$B_1 = r_{13}F_1, \quad r_{13} = \frac{r_{12} + r_{23}e^{i\delta}}{1 - r_{23}r_{21}e^{i\delta}}, \tag{5b}$$

where we have applied the Stokes' identity $t_{12}t_{21} + r_{12}^2 = 1$. Using the fact that $r_{12} = -r_{21}$, we can see that these formulas give the standard reflection and transmission coefficients of a Fabry-Perot resonator.

3. Multiple isotropic layers

We now build on the ideas of a three layer system to find the effective coefficients of an N layer system. To do so, we consider the system of N layers as a 3 layer system, replacing the layers 3 to $N-1$ with an effective boundary between layers 2 and N. This is depicted in figure 1(c), where a jagged line indicates an effective boundary. Applying the same methodology as before, we derive the effective coefficients of the N layer system as

$$t_{1N} = \frac{t_{12}t_{2N}e^{i\frac{\delta_2}{2}}}{1 - r_{2N}r_{21}e^{i\delta_2}}, \tag{6a}$$

$$r_{1N} = \frac{r_{12} + r_{2N}e^{i\delta_2}}{1 - r_{2N}r_{21}e^{i\delta_2}}, \tag{6b}$$

where we have written the phase difference as δ_2 to make clear that it depends on the refractive index and thickness of layer 2. To calculate the coefficients from layer 1 to N we must know the effective coefficients from layer 2 to N, which will in turn require the effective coefficients from layer 3 to N, and so on. This means that the coefficients can be built recursively, working *backwards* from the final layer.

To calculate the effective coefficients between two general layers j and k, we consider the same configuration as in figure 1(c), but replace the layers 1, 2, and N with j, $j+1$, and k, respectively.

We can then write that, for any j and k in our N layer system (excluding $|j-k|<2$, in which case we just need the regular Fresnel coefficients)

$$t_{jk} = \frac{t_{j,j+1}t_{j+1,k}e^{i\frac{\delta_{j+1}}{2}}}{1-r_{j+1,k}r_{j+1,j}e^{i\delta_{j+1}}}, \tag{7a}$$

$$\begin{aligned} r_{jk} &= r_{j,j+1} + \frac{t_{j,j+1}r_{j+1,k}t_{j+1,j}e^{i\delta_{i+1}}}{1-r_{j+1,k}r_{j+1,j}e^{i\delta_{j+1}}} \\ &= \frac{r_{j,j+1}+r_{j+1,k}e^{i\delta_{i+1}}}{1-r_{j+1,k}r_{j+1,j}e^{i\delta_{j+1}}} \end{aligned} \tag{7b}$$

if we are traveling forwards, i.e. $j<k$. If we are traveling backwards, that is, $j>k$,

$$t_{jk} = \frac{t_{j,j-1}t_{j-1,k}e^{i\frac{\delta_{j-1}}{2}}}{1-r_{j-1,k}r_{j-1,j}e^{i\delta_{j-1}}}, \tag{8a}$$

$$r_{jk} = \frac{r_{j,j-1}+r_{j-1,k}e^{i\delta_{i-1}}}{1-r_{j-1,k}r_{j-1,j}e^{i\delta_{j-1}}}. \tag{8b}$$

In both cases, by working iteratively backwards from the final layer, the only terms that appear are the effective transmission and reflection calculated at the previous iteration, and the regular Fresnel coefficients for the new boundary that is added at each step. One simply needs to start with $r_{k-2,k}$ and $t_{k-2,k}$ and work back to r_{jk} and t_{jk} by using equations (7) and (8) for forward and backward travel, respectively.

Finally, we can also evaluate the forwards and backwards fields in each layer. To find the forwards and backwards fields F_i and B_i in layer i, we once again consider the N layer system as a 3 layer system. By replacing layers 2 to $i-1$ with an effective interface between layers 1 and i, and replacing layers $i+1$ to $N-1$ with an effective interface between layers i and N, we can see that we must have that

$$F_N = t_{iN}F_i \quad \text{and} \quad B_i = r_{iN}F_i. \tag{9}$$

On the other hand, we also know that $F_N = t_{1N}F_1$, from which it follows that

$$F_i = \frac{t_{1N}}{t_{iN}}F_1, \tag{10a}$$

$$B_i = \frac{t_{1N}r_{iN}}{t_{iN}}F_1. \tag{10b}$$

4. Transmission and reflection of anisotropic layers

4.1. General multi-mode formalism

So far we have only considered systems of isotropic media. There is no polarisation rotation upon transmission and reflection and all rays have the same tangential wave vector component. As a result, all of these rays can be thought of as a single mode of the system, and the iterated ray method is a scalar calculation. In general, however, a system may possess distinct modes that mix with one another. In the presence of anisotropic media, for example, the o- and e-waves, with distinct polarisation states and directions of propagation, must be considered separately. Alternatively, there may be a layer that acts as a diffracting element, in which case there will be mixing between diffracted orders that must also be considered separately. We therefore generalize the scalar method of the previous section to account for mode mixing.

We first define the mode vectors in each layer n as $\boldsymbol{F}^{(n)}$ and $\boldsymbol{B}^{(n)}$ for the forward and backward fields, respectively. The i'th component of the vectors gives the total field of the i'th mode in layer

n, i.e., $F_1^{(n)}$ is the sum of all the forward traveling rays of mode type 1 in layer n, etc.. The number of components is therefore equal to the number of independent modes in the corresponding layer, e.g. 1 for an isotropic medium and 2 for a birefringent material.

We assume that the modes in each layer are known, and also that we know the various coefficients describing their transmission and reflection at their layer boundaries. The effective transmission and reflection from layer j to k of the various modes are then derived in the same manner as the isotropic case, equations (7) and (8), with scalar quantities replaced by matrices. For a system of m modes they are

$$\mathrm{T}_{jk} = \mathrm{T}_{j+1,k}\left[\mathit{I} - \Phi^+_{j+1}\mathrm{R}_{j+1,j}\Phi^-_{j+1}\mathrm{R}_{j+1,k}\right]^{-1}\Phi^+_{j+1}\mathrm{T}_{j,j+1}, \tag{11a}$$

$$\mathrm{R}_{jk} = \mathrm{R}_{j,j+1} + \mathrm{T}_{j+1,j}\left[\mathit{I} - \Phi^-_{j+1}\mathrm{R}_{j+1,k}\Phi^+_{j+1}\mathrm{R}_{j+1,j}\right]^{-1}\Phi^-_{j+1}\mathrm{R}_{j+1,k}\Phi^+_{j+1}\mathrm{T}_{j,j+1}. \tag{11b}$$

Here I represents the $m \times m$ identity matrix. The matrices T_{ij} and R_{ij} are also $m \times m$, and they contain the transmission and reflection coefficients of the modes going from layer i to layer j. The kl element $\left(\mathrm{T}_{ij}\right)_{kl}$ is the transmission of the k'th mode to the l'th mode going across layers i to j (and similarly for the R matrices). The matrices Φ^+_i and Φ^-_i contain the phase changes of the modes going across layer i in the forwards and backwards direction, respectively. These phase changes are not, in general, the same, since the forwards and backwards waves in an anisotropic layer have different refractive indices and normal wave vector components. While the Φ matrices are always diagonal the T and R matrices are only diagonal when they correspond to an isotropic–isotropic interface.

To increase computational efficiency, we note that the above equations can be rewritten as

$$\mathrm{T}_{jk} = \mathrm{T}_{j+1,k}\mathrm{L}_{j+1}\mathrm{T}_{j,j+1}, \tag{12a}$$

$$\mathrm{R}_{jk} = \mathrm{R}_{j,j+1} + \mathrm{T}_{j+1,j}\Phi^-_{j+1}\mathrm{R}_{j+1,k}\mathrm{L}_{j+1}\mathrm{T}_{j,j+1}, \tag{12b}$$

where

$$L_{j+1} = \left[\mathit{I} - \Phi^+_{j+1}\mathrm{R}_{j+1,j}\Phi^-_{j+1}\mathrm{R}_{j+1,k}\right]^{-1}\Phi^+_{j+1} \tag{12c}$$

is the layer matrix for layer $j+1$. The layer matrix takes a forward field at the $j, j+1$ boundary and creates the total forward field at the $j+1, k$ effective boundary that results from all of the reflections of the initial field. $\mathrm{L}_{j+1}\mathrm{T}_{j,j+1}$ is then the total forward field at the $j+1, k$ effective boundary, arising from field incident on the layered structure from layer j. Intuitively, the total transmission is then found simply by multiplying this with $\mathrm{T}_{j+1,k}$, while the reflection is found by reflecting, propagating, and transmitting back into layer j (and of course adding the contribution from the initial external reflection, $\mathrm{R}_{j,j+1}$).

Common with existing S-matrix methods, we note that the calculation of R_{jk} is independent of T_{jk}. This means that if only the reflection from the layered structure is desired, we need only calculate the effective reflection at each iteration. This is known as the quarter matrix recursion in S-matrix terminology (since we are only calculating one of the four S-parameters). If T_{jk} is desired, which depends on R_{jk}, then both must be calculated, known as the half matrix recursion. If either T_{kj} or R_{kj} is required, then we must perform the full matrix recursion. The effective coefficients in the backwards direction can be obtained using

$$\mathrm{R}_{kj} = \mathrm{R}_{k,j+1} + \mathrm{T}_{j+1,k}\mathrm{L}_{j+1}\mathrm{R}_{j+1,j}\Phi^-_{j+1}\mathrm{T}_{k,j+1} \tag{12d}$$

$$\mathrm{T}_{kj} = \mathrm{T}_{j+1,j}\left[\mathit{I} + \Phi^-_{j+1}\mathrm{R}_{j+1,k}\mathrm{L}_{j+1}\mathrm{R}_{j+1,j}\right]\Phi^-_{j+1}\mathrm{T}_{k,j+1} \tag{12e}$$

We also note that, in analogy with equations (10), this formulation allows us to describe the fields within each layer by

$$\boldsymbol{F}^{(i)} = \mathrm{T}^{-1}_{iN}\mathrm{T}_{1N}\boldsymbol{F}^{(1)} \quad \text{and} \quad \boldsymbol{B}^{(i)} = \mathrm{R}_{iN}\mathrm{T}^{-1}_{iN}\mathrm{T}_{1N}\boldsymbol{F}^{(1)}. \tag{13}$$

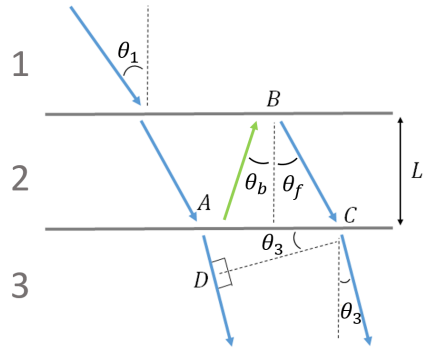

Fig. 2. Calculation of the optical path length difference between two subsequent transmitted or reflected rays in a birefringent medium. The incident and reflection angles, θ_f and θ_b, are in general not equal.

4.2. A single anisotropic layer

As an example application of the multi-mode formulas derived in the previous section, we now consider the case of a uniaxial anisotropic material bounded by isotropic media, and derive in full the transmission and reflection coefficients. We represent the input and output fields in terms of their s and p components, and so we first look to write

$$\begin{pmatrix} F_p^{(3)} \\ F_s^{(3)} \end{pmatrix} = \mathrm{T}_{13} \begin{pmatrix} F_p^{(1)} \\ F_s^{(1)} \end{pmatrix}. \tag{14}$$

We will chose the first mode in the uniaxial layer to be the ordinary rays (indicated by the suffix o) and the second mode to be the extraordinary rays (indicated by the suffix e), that is,

$$\boldsymbol{F}^{(2)} = \begin{pmatrix} F_o^{(2)} \\ F_e^{(2)} \end{pmatrix} \quad \text{and} \quad \boldsymbol{B}^{(2)} = \begin{pmatrix} B_o^{(2)} \\ B_e^{(2)} \end{pmatrix}. \tag{15}$$

Using equations (12a) and (12c), the transmission matrix is then found to be

$$\mathrm{T}_{13} = \begin{pmatrix} t_{op}^{23} & t_{ep}^{23} \\ t_{os}^{23} & t_{es}^{23} \end{pmatrix} \boldsymbol{F}^{(2)} \tag{16}$$

where

$$\boldsymbol{F}^{(2)} = [\mathcal{I} - \mathrm{R}]^{-1} \begin{pmatrix} t_{po}^{12} e^{iq_o^+ L} & t_{so}^{23} e^{iq_o^+ L} \\ t_{pe}^{12} e^{iq_e^+ L} & t_{se}^{12} e^{iq_e^+ L} \end{pmatrix} \tag{17}$$

and

$$\mathrm{R} = \begin{pmatrix} r_{oo}^{23} r_{oo}^{21} e^{i(q_o^+ - q_o^-)L} + r_{oe}^{23} r_{eo}^{21} e^{i(q_o^+ - q_e^-)L} & r_{eo}^{23} r_{oo}^{21} e^{i(q_o^+ - q_o^-)L} + r_{ee}^{23} r_{eo}^{21} e^{i(q_o^+ - q_e^-)L} \\ r_{oe}^{23} r_{ee}^{21} e^{i(q_e^+ - q_e^-)L} + r_{oo}^{23} r_{oe}^{21} e^{i(q_e^+ + q_o^+)L} & r_{ee}^{23} r_{ee}^{21} e^{i(q_e^+ - q_e^-)L} + r_{eo}^{23} r_{oe}^{21} e^{i(q_e^+ + q_o^+)L} \end{pmatrix}. \tag{18}$$

The symbols $r_{\alpha\beta}^{ij}$ and $t_{\alpha\beta}^{ij}$ are the Fresnel reflection and transmission coefficients between the modes α and β in layers i and j, with α and β equal to s or p in the isotropic layers, $j \in \{1, 3\}$,

or o and e in the uniaxial layer, $j = 2$. Finally, the symbols $q_\alpha^\pm$ are the normal components of the wave vector for the α mode in the forward (+) or backward (−) direction. The phase shift terms in R_t are found by considering figure 2, where the forward and backwards rays are described by their angles θ_f and θ_b, and by their refractive indices n_f and n_b. In general, the path difference is given by

$$\begin{aligned}\delta &= k_0 \left[\left|\overrightarrow{AB}\right| n_b + \left|\overrightarrow{BC}\right| n_f - \left|\overrightarrow{AD}\right| n_3 \right] \\ &= k_0 L \left[n_b \sec(\theta_b) + n_f \sec(\theta_f) - n_3 \left|\sin(\theta_3)\right| \left(\left|\tan(\theta_b)\right| + \left|\tan(\theta_f)\right| \right) \right] \qquad (19) \\ &= \left(q_f - q_b \right) L, \qquad (20)\end{aligned}$$

where we have used Snell's law to simplify the last step. With the same notation used in equation (18), q_f and q_b are the normal components of the wave vectors of the forward and backward rays, respectively. This formula is used in equation (18) for the four possible permutations of a backwards ordinary/extraordinary wave reflecting back as a forwards ordinary/extraordinary wave.

Similarly, using equation (12b), the reflection coefficient R_{13} from the anisotropic layer, defined by

$$\begin{pmatrix} B_p^{(1)} \\ B_s^{(1)} \end{pmatrix} = \mathrm{R}_{13} \begin{pmatrix} F_p^{(1)} \\ F_s^{(1)} \end{pmatrix}, \qquad (21)$$

is given by

$$\mathrm{R}_{13} = \begin{pmatrix} r_{pp}^{12} & r_{sp}^{12} \\ r_{ps}^{12} & r_{ss}^{12} \end{pmatrix} + \begin{pmatrix} t_{op}^{21} & t_{ep}^{21} \\ t_{os}^{21} & t_{es}^{21} \end{pmatrix} \begin{pmatrix} r_{oo}^{23} e^{-iq_o^- L} & r_{eo}^{23} e^{-iq_o^- L} \\ r_{oe}^{23} e^{-iq_e^- L} & r_{ee}^{23} e^{-iq_e^- L} \end{pmatrix} \boldsymbol{F}_2 \qquad (22)$$

The transmission and reflection for backward travel are given by interchanging all superscript 1's and 3's and changing all $q_\alpha^\pm$ to $-q_\alpha^\mp$.

We emphasize that in this anisotropic case, although the method presented in this paper is known as the Iterated Ray Method, it is the wave vectors that must be used to calculate the various fields. In anisotropic media the extraordinary rays (which are in the direction of the Poynting vectors) and their wave vectors are not parallel, and it is the directions of the wave vectors that must be used in Snell's law and to calculate the various Fresnel coefficients.

The full procedure for obtaining the directions of propagation and the Fresnel coefficients is described in the Supplemental document. A graphical interpretation of the extension of Snell's law to anisotropic media is shown in figure 3 for the case that the optical axis $\boldsymbol{c}$ is in the plane of incidence (though the equations and methodology presented in this paper are general and apply to any orientation of $\boldsymbol{c}$). The method relies on the use of the so-called wave normal surfaces, which describe the orientation and magnitude of the wave vectors that are solutions of Maxwell's equations in a given medium, and on the continuity of the tangential component of wave vectors at a material discontinuity. The directions of propagation of the various waves in the anisotropic layer are used to find the corresponding electric fields, and the usual electromagnetic boundary conditions are used to find the Fresnel coefficients. A more detailed explanation of the wave normal surfaces and their derivation, along with the calculation of the electric fields, can be found in [22].

5. Multiple anisotropic layers

The procedure for modeling a single anisotropic layer, outlined in the Supplemental document, is fully analytic, and the Fresnel coefficients are derived by hand. In the case of multiple, neighboring anisotropic layers, while the procedure to find the normalized fields in each anisotropic layer is exactly as in section 1 of the Supplemental document, the algebra required to find the Fresnel

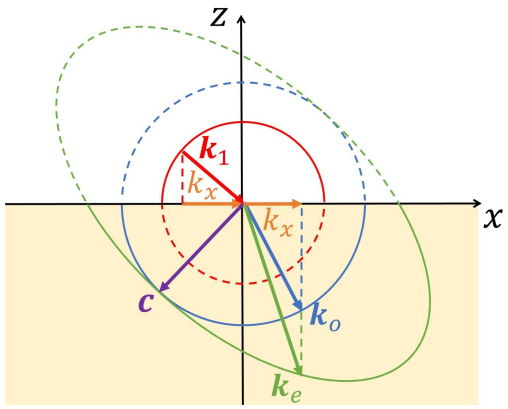

Fig. 3. A graphical interpretation of the wave normal calculations at an interface between an isotropic (top) and an anisotropic (bottom) layer shown in the plane of incidence. The red circle is the wave normal surface in medium 1, and $\boldsymbol{k}_1$ is the incident wave vector. The tangential wave vector component k_x (orange) must be conserved across the boundary, and there are two possible waves in medium 2 that satisfy this. The first is the ordinary wave, with wave vector $\boldsymbol{k}_o$ lying on the ordinary wave normal surface (blue circle). The second is the extraordinary wave, with wave vector $\boldsymbol{k}_e$ lying on the extraordinary wave normal surface (green ellipse). The vector $\boldsymbol{c}$ is the optical axis of the medium and also the minor axis of the extraordinary wave normal surface [22].

coefficients will be more intensive, and we now highlight how the necessary coefficients can easily be found numerically through a matrix method. We take the layer normals to be parallel to the z axis, the plane of incidence to be the xz plane, and the wave vector of each wave $\boldsymbol{E}^\alpha$ is $\boldsymbol{k}_\alpha = k_0\left(K, 0, \sqrt{n_\alpha^2 - K^2}\right)$. The boundary conditions that need to be satisfied are the continuity of E_x, E_y, $\partial_z E_y$, and $\partial_z E_x - iKE_z$. Considering, for instance, the case of an o-wave incident upon the boundary from the first anisotropic medium to the second, the boundary conditions can be written as

$$\begin{pmatrix} E_x^{o+} \\ E_y^{o+} \\ q_{o+}E_x^{o+} \\ C^{o+} \end{pmatrix} = \begin{pmatrix} -E_x^{o-} & -E_x^{e-} & \tilde{E}_x^{o+} & \tilde{E}_x^{e+} \\ -E_y^{o-} & -E_y^{e-} & \tilde{E}_y^{o+} & \tilde{E}_y^{e+} \\ -q_{o-}E_y^{o-} & -q_{e-}E_y^{e-} & \tilde{q}_{o+}\tilde{E}_y^{o+} & \tilde{q}_{e+}\tilde{E}_y^{e+} \\ -C^{o-} & -C^{e-} & \tilde{C}^{o+} & \tilde{C}^{e+} \end{pmatrix} \begin{pmatrix} r_{oo}^{12} \\ r_{oe}^{12} \\ t_{oo}^{12} \\ t_{oe}^{12} \end{pmatrix}, \tag{23}$$

where

$$C^{o+} = q_{o+}E_x^{o+} - KE_z^{o+} \tag{24}$$

and a tilde denotes that it is the electric field/wave vector component in the second medium. Denoting the vector

$$\boldsymbol{v}^\alpha = \begin{pmatrix} E_x^\alpha & E_y^\alpha & q_\alpha E_x^\alpha & C^\alpha \end{pmatrix}^T, \tag{25}$$

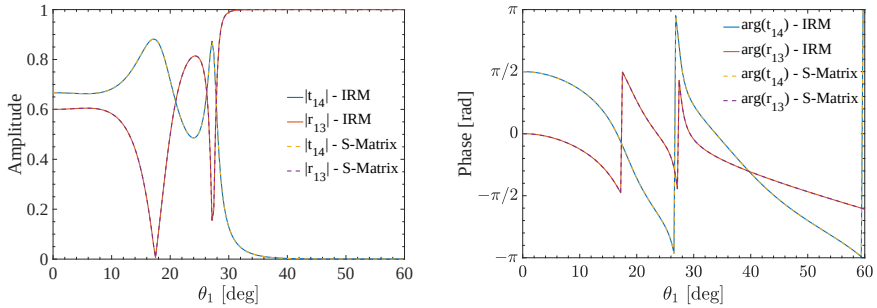

Fig. 4. (Left) The amplitude of the transmission across a four layer system and reflection from the initial three layer subsystem. (Right) The corresponding phase of the transmission and reflection coefficients. The layer refractive indices are $n_j = \{2, 1, 2, 2.5\}$, for j increasing from 1 to 4. The thicknesses of the second and third layers are 1.5 and 0.5 wavelengths respectively.

we can consider the cases of each of the four waves incident upon the anisotropic/anisotropic boundary to write out the four sets of four boundary conditions as

$$\begin{pmatrix} \boldsymbol{\nu}^{o+} & \boldsymbol{\nu}^{e+} & \tilde{\boldsymbol{\nu}}^{o-} & \tilde{\boldsymbol{\nu}}^{e-} \end{pmatrix} = \begin{pmatrix} -\boldsymbol{\nu}^{o-} & -\boldsymbol{\nu}^{e-} & \tilde{\boldsymbol{\nu}}^{o+} & \tilde{\boldsymbol{\nu}}^{e+} \end{pmatrix} \begin{pmatrix} r_{oo}^{12} & r_{eo}^{12} & -t_{oo}^{21} & -t_{eo}^{21} \\ r_{oe}^{12} & r_{ee}^{12} & -t_{oe}^{21} & -t_{ee}^{21} \\ t_{oo}^{12} & t_{eo}^{12} & -r_{oo}^{21} & -r_{eo}^{21} \\ t_{oe}^{12} & t_{ee}^{12} & -r_{oe}^{21} & -r_{ee}^{21} \end{pmatrix}. \tag{26}$$

The Fresnel coefficients can be found from the obvious matrix inversion, with the necessary matrices for the Iterated Ray Method given by

$$\begin{pmatrix} \mathrm{R}_{j,j+1} & -\mathrm{T}_{j+1,j} \\ \mathrm{T}_{j,j+1} & -\mathrm{R}_{j+1,j} \end{pmatrix} = \begin{pmatrix} -\boldsymbol{\nu}^{o-} & -\boldsymbol{\nu}^{e-} & \tilde{\boldsymbol{\nu}}^{o+} & \tilde{\boldsymbol{\nu}}^{e+} \end{pmatrix}^{-1} \begin{pmatrix} \boldsymbol{\nu}^{o+} & \boldsymbol{\nu}^{e+} & \tilde{\boldsymbol{\nu}}^{o-} & \tilde{\boldsymbol{\nu}}^{e-} \end{pmatrix}, \tag{27}$$

to be substituted straight into equations (12a) to (12c).

6. Numerical validation

We have validated the Iterated Ray Method by comparing its results with the gold standard in light propagation methods in layered media, the S-matrix algorithm [20]. We have focused on structures that have evanescent waves in internal layers because these are well known to have the potential to give rise to numerical instabilities.

The stability of the ray method is evident from equations (7) and (8). There are only forward propagating exponential terms. Therefore, in the presence of evanescent fields, the coefficients display only exponential decay, never growth as in the T-matrix method [20]. The stability of the method and its accuracy are evidenced by the example in figure 4. We observe the total internal reflection across the evanescent layer (layer 2 with refractive index 1) at approximately 30°, shown by $|r_{13}|$ going to one. Correspondingly, we see the transmission across the entire system, $|t_{14}|$, go to zero. The agreement between the Iterated Ray method and the S-matrix is to numerical precision, both in modulus and phase (left and right panels of figure 4 respectively).

To validate the anisotropic formulas we have compared the output of equations (16) and (22) with the output of a finite elements simulation of the three layers, implemented in Comsol. The

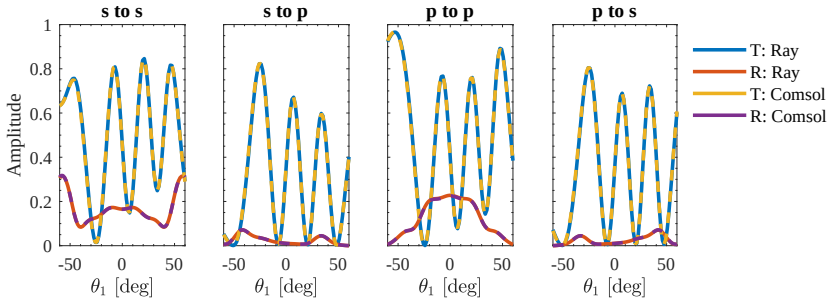

Fig. 5. A comparison of the modulus of the various transmittances, T, and reflectances, R, for s- and p-polarized incident fields to s- and p-polarized output fields. The system refractive indices are $n_{in} = 1$, $n_e = 5$, $n_o = 1.5$, and $n_{out} = 2$. The layer thickness is two wavelengths and the optical axis is at an angle of $\pi/3$ with the y axis, with its projection in the xz plane (plane of incidence) equal to $\pi/5$. The z axis is perpendicular to the plane of the layers.

model consists of a 2D rectangular geometry made up from five layers. These are the three layers considered in the Iterated Ray method sandwiched between perfectly matched layers (PMLs). The PMLs are near perfectly absorbing until high angles of incidence and prevent any non-physical resonance effects being observed. The electric field is then solved for using the electromagnetic waves module, subject to Floquet periodic boundary conditions to simulate a plane wave incident on an infinitely extending layer. In figure 5 we plot the transmittance, $T = |t_{13}|^2 n_3 \cos(\theta_3)/(n_1 \cos(\theta_1))$ and the reflectance, $R = |r_{13}|^2$, computed using the two methods. The layer is highly anisotropic and asymmetric with respect to the angle of incidence so as to induce very large, asymmetric polarization rotation effects for the purposes of comparison; the agreement between the two is exact to the precision of the finite element simulation. The agreement in the phase of the emerging waves is to the same level of accuracy. The graphs depicting this are omitted, however, as they are highly oscillatory and hard to show in clear enough detail with limited space.

7. Computational efficiency

We now consider the efficiency of the Iterated Ray Method and its comparison with existing S-matrix methods, where we have found that the Iterated Ray Method compares favorably in speed with respect to the S-matrix method. It is arguably hard to compare different algorithms as the speed of a code depends on many factors, such as the number of floating point operations, vectorization and memory requirements. We have taken two approaches to compare the two methods. In the first one, we have coded equations (6a) and (6b) and the S-matrix algorithm (as originally presented in [20]) in Matlab, and have optimized their performance to the best of our abilities. We have run the two codes on a large sample of random, isotropic, layered structures (in terms of layer thicknesses and refractive indices), for a large range of number of layers (3-20) and number of angles of incidence/modes (10-1000). The Iterated Ray Method code was between 25 and 65 times faster than the S-matrix code, with the larger increases of speed found for larger numbers of incident angles/modes; fixing the number of incident angles and increasing the number of layers did not noticeably affect the speed increase.

This approach, while holistic, suffers from the drawback of being affected by our coding of the two algorithms. It must also be considered that there are many different formulations of the S-matrix algorithm, each with different running speeds. Handily, Li [25,26] has already presented a detailed a comparison of the various versions of the S- (and R-) matrix algorithms, including a

count of the floating point operations required by each to run. This is done for the quarter, half, and full recursions discussed in section 4.1. The algorithms account for mode mixing (in the setting of layered diffraction gratings where the different modes are described by their tangential wave vector components), and for N modes the recursion formulas are constructed from N by N matrices. Li therefore counts the number of floating point operations that are of largest order ($O(N^3)$), such as matrix multiplications and inversions, and matrix additions are ignored. The fastest methods, in the notation of Li, are the $W \to S$ and $W \to t \to S$ variants, depending on whether a certain symmetry in the boundary condition matrices (the W's) can be exploited.

Considering first the case of layered isotropic media where there is no mode mixing, the matrices in all S-matrix variants become diagonal. The order of the matrix multiplications is only $O(N)$ in this case, which is the same as additions. We have therefore repeated the counting process for this isotropic case, where the W symmetry can also be exploited for faster computation, and counted the total number of real floating point operations (remembering that the multiplication of two complex numbers requires four multiplications and two additions etc) required per layer per mode, the results of which are shown in table 1.

Algorithm	Operation Counts		
	Quarter	Half	Full
$W \to S$	53	59	107
$W \to t \to S$	48	60	100
Iterated Ray Best	31	45	60
Iterated Ray Worst	38	50	75

Table 1. The total number of floating point operations required per layer per mode to compute the various effective Fresnel coefficients/S-parameters for a layered isotropic structure.

The listed number of operations required by the Iterated Ray Method (equations (7b) to (8b) and the calculation of the isotropic/isotropic Fresnel coefficients) covers the best and worst possible cases. The calculation of the p-polarized Fresnel coefficients requires a few more multiplications than the s-polarized, and an evanescent field makes for a greater number of operations in the recursion formulas owing to the fact that the Fresnel coefficients become complex. Thus, the best case covers the addition of a layer with an s-polarized propagating field, and the worst case covers the addition of a layer with a p-polarized evanescent field. Even in the worst case, we see that the Iterated Ray Method requires around 15%-25% fewer operations, again confirming that the iterated Ray Method is a computationally efficient algorithm.

In terms of the Iterated Ray Method applied to anisotropic media, we can apply the counting methodology of Li to count the number of $O(N^3)$ matrix operations performed in the calculation of equations (27) and (12a) to (12e). The operation counts are found to be 15, 16, and 64/3 for the quarter, half, and full matrix recursions, respectively. These are in exact agreement with the counts for the $W \to s \to \tilde{s} \to S$ variant of the S-matrix given in [25], the third fastest of the algorithms (sitting behind the second place $W \to t \to S$ variant by only a small margin). This is maybe unsurprising given that we could describe the Iterated Ray Method as a $W' \to s \to S$ variant, where we use W' to distinguish that the boundary condition matrices are different to those in [25], relating the various components of the normalised o- and e-fields, rather than relating the amplitudes of the various up and down diffracted orders. While it is unclear if a $W' \to S$ variant for the anisotropic problem exists, and if this would also be the fastest variant (an interesting possibility for future exploration), given the results of Li it seems likely that the

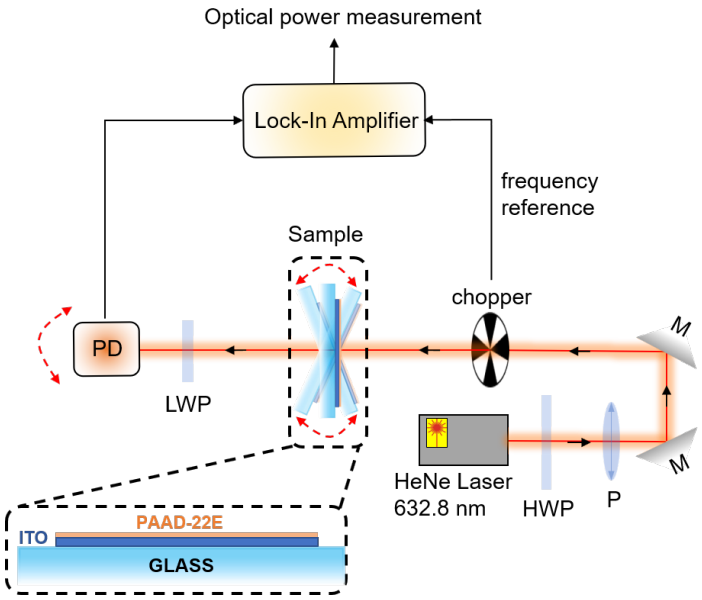

Fig. 6. Experimental setup to measure the transmittance coefficients as a function of the angle of incidence, of PAAD-22E isotropic thin film, $T(\theta_1)$. A HeNe laser was used at 632.8 nm wavelength and 1.4 mW power as measured at the surface of the sample. The polarization of the incident light beam was controlled through a half wave-plate (HWP) and a polarizer (P). To reject background noise, we used a lock-in amplifier, where an optical chopper modulated the signal. A long wave pass trim filter (LWP) helped further into cutting down the unwanted signals.

Iterated Ray Method provides one of the most efficient means to solve the anisotropic problem.

8. PAAD thin film refractive index measurement

Photo-aligning azobenzene dyes (PAADs) are known to exhibit strong, selective photo-sensitivity due to their capability to convert efficiently between their trans and cis states when subjected to UV and visible light illumination [27–31]. Upon irradiation, the PAAD molecules undergo a realignment process. In thicker layers it is known that this results in all of the molecules being oriented perpendicularly to the polarization of light [32–34]. Therefore, optically controlled films of such PAAD layers can form high resolution patterns, enabling their use for polarization gratings and spiral phase liquid crystal wave-plates [35–37], and to be effective in the photo-alignment of liquid crystals [35, 36, 38–42]. However, despite their extensive use, the optical properties of *thin* PAAD layers are not yet fully understood.

We have used the Iterated Ray Method to obtain the intrinsic properties (i.e. refractive index and film thickness) of isotropic PAAD layers in their unaligned state. The material that we investigated in this work has the commercial name PAAD-22E (BEAM Co.), with two absorbance peaks at 375 nm and 440 nm [30]. Thin films of PAAD-22E dyes were fabricated by dissolving the dye powder in methanol at a concentration of 1% g/ml, and sonicated for 5 minutes until a transparent solution was obtained. Thin films were then deposited on ITO covered glass substrates by spin coating at 3000 rpm. After deposition, the films were annealed on a hot plate for 10 minutes at 90 °C. In our experiments we used 1 mm thick glass substrates.

To monitor the transmittance of incident light through the samples, a HeNe laser at 632.8 nm and 1.4 mW was used as a probe. The choice of the probe wavelength was due to the low

absorption of the PAAD films at 632.8 nm, minimizing any realignment effects as the probe passes through the PAAD-22E films. The polarization of the probe was controlled with the aid of a polarizer (P) and a half wave plate (HWP), as depicted in figure 6. Finally, with the aid of two mirrors (M), we controlled and focused the beam on the sample.

The incident angle and polarization of the probe beam was varied to monitor the transmittance of the s- and p-polarized outputs. In order to achieve this, the sample was held in rotation stage. The stage consists of a 360 degree rotating base, with a holder to keep the sample centered on the stage's rotational axis (as depicted in figure 6, the axis points out of the page). In this way, the incident light remained focused on the same spot of the sample as the stage was rotated, enabling us to monitor the transmission of the same spot of the sample for all of the different angles of incidence (depicted by the red dashed arrows around the sample in figure 6). After propagating through the sample, the transmitted light was collected by a photo-diode (PD), measuring its intensity.

In order to remove background noise we used a lock-in amplifier and an optical chopper. The amplifier increased the signal to noise ratio and the chopper was used to modulate the signal and provide a reference frequency. Further unwanted background signals were then filtered with a long wave pass trim filter (LWP) before the PD. The experiment was fully controlled by Matlab software, performing experimental apparatus control, data acquisition, and subsequent data normalization with respect to the reference data. Finally, to reduce the experimental noise, we also averaged the data points at opposite incident angles, as the transmission across isotropic layers is symmetric about normal incidence.

To form the theoretical model for comparison with the experimental results, the Iterated Ray method was applied to the five layer system (air/PAAD-22E/ITO/glass/air) to calculate the transmittance as a function of the angle of incidence. The refractive indices and thicknesses of the PAAD and ITO layers were unknown, and are the four fitting parameters used in the fitting/optimization routine.

This did not form the entire model, however. From standard Fabry-Perot theory, and that of the Iterated Ray Method, we see that the large thickness of the glass layer (approx. 1 mm) induces many rapid oscillations of the transmitted intensity as a function of the incidence angle. This is the case, at least, for an incident plane wave. In the experimental data, however, the oscillations are averaged out by the filtering caused by the finite size and coherence of the Gaussian laser beam. It was therefore also necessary to smooth the theoretical transmission data $T(\theta_1)$ using a Gaussian filter, calibrated by fitting the transmission data of single glass slide. We note that the resonant effects of the glass are still evident in the narrow region near normal incidence (see the small sharp peaks in the experimental transmitted intensity visible in figure 7). In this region the phase difference between neighboring, emerging rays (and hence the overall transmission) varies with angle of incidence on a far slower scale, and, consequently, the averaging is less effective.

The Iterated Ray solution plus the Gaussian averaging formed the complete theoretical model. This model was used in a Matlab minimization routine to fit to the experimental data and obtain values for the unknown refractive indices and thicknesses. In the fitting process we excluded the data points for incident angles larger than $\pm 56^\circ$ due to the steep slope of the data. The steep slopes meant that, while the experimental and theoretical curves could be very close to one another, the errors between the two in the least squares sense (difference vertically) could lead to enormous errors and make successful fitting impossible. We also ran the fitting in two stages, fitting first the larger angles of incidence for the PAAD and ITO parameters, and then fine tuning the glass thickness to fit the center region where the glass resonance effects were observable.

The experimental and best fit curves are shown in figure 7, and the fitted parameters are shown in table 2. The ITO thickness given by the fitting process is consistent with the specifications of ITO/glass substrates offered by many manufacturers, usually in the 100-200 nm range. The refractive index is also in good agreement with values in the literature, e.g 1.87 [43] and 1.78 [44].

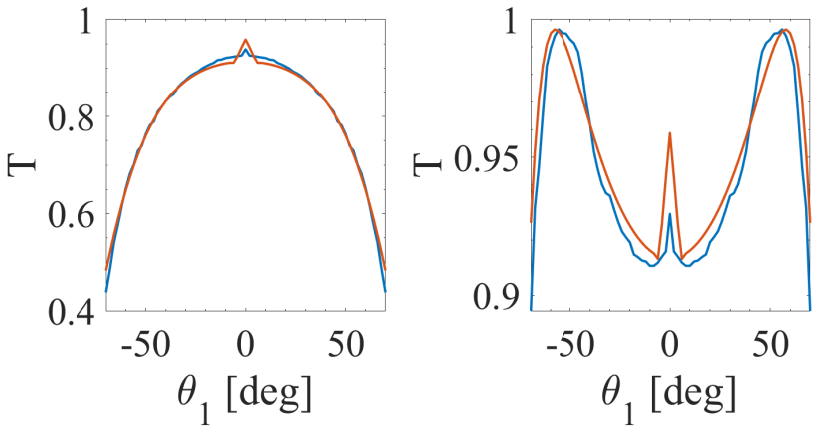

Fig. 7. Graphs showing the experimental (blue) and fitted (orange) transmission curves for an s-polarized (left) and p-polarized (right) 632.8 nm beam incident onto the PAAD/ITO/glass system.

The thickness and refractive index of the PAAD-22E layer are consistent with the values of 45 ± 20 nm and 1.8 ± 0.1 found in [30], in which samples created with the same methodology were studied, and the thickness and refractive index were found using profilometry and ellipsometry, respectively.

Material	Ref. Index	Thickness [nm]
PAAD-22E	1.73	27
ITO	1.85	142

Table 2. Refractive index and thickness of a PAAD-22E and ITO layers deposited on a glass slide obtained by fitting the experimental data in figure.

Before concluding this section, we would like remark that the PAAD film analyzed here was placed on a glass substrate that contributed significantly to the shape of the transmitted light intensity. This is a different geometry from ellipsometry studies, which are instead based in detecting polarization changes in the light reflected by the thin film. The aim of the experiment examined here was to analyze the PAAD film on the same type of substrate and conditions in which it would be used once in a liquid crystal cell, wave plate, or other component. Our analysis is, thus, inspecting a more realistic and practical photo-alignment system. This imposed severe constraints on the fitting procedure because of the need to average over the multiple Fabry-Perot resonances in the glass substrate. We have used a very fine angular resolution of around $0.04°$ to capture the oscillations of the theoretical transmission and ensure the convergence of the averaging process. The fact that we have been able to do this on a standard desktop in a reasonable time is a further confirmation of the computational efficiency of the Iterated Ray Method.

9. Conclusion

The Iterated Ray Method is a highly efficient and accurate algorithm to compute the reflection and transmission coefficients of layered structures. It is based on the intuitive picture of rays being partially transmitted and reflected at each interface and uses series sums of each reflection and transmission coefficient to build an efficient recursive algorithm for the total reflectance

and transmittance of the multi-layered structure. The associated coding of the algorithm is straightforward and a sample code for isotropic and anisotropic media is available from Code 1, [24]. The Iterated Ray Method code is very efficient and has the potential of speeding up considerably beam propagation and refractive index optimization in multi-layered structures, which should be particularly beneficial for more complex structures with anisotropic layers.

We have tested its accuracy and reliability against numerical simulations for both propagating and evanescent waves. Its results are identical to *S*-matrix and finite element simulations, for both isotropic and anisotropic media, respectively. In this paper we have focused on the application of the Iterated Ray Method to the determination of the refractive index and thickness of thin films of interest for photo-addressable liquid crystal devices, and have obtained very good agreement with literature values. The method, however, is of general use, and could be applied, for example, to the optimization of Bragg gratings in wave guides or film coatings on surfaces. Finally, the Iterated Ray Method, in common with other layered structured algorithms, assumes that the electromagnetic field is a plane wave. This, however, is not a strong constraint on the method. Coupling its efficient handling of plane waves with the angular spectrum (plane wave decomposition) of an electromagnetic field should yield a computationally efficient and general method for light propagation through locally flat layered media.

Acknowledgments

We wish to thank Nelson Tabiryan (Beam Co.) for providing us with PAAD samples and Marina Grenzer (Saphiannikova) (Institute Theory of Polymers, Dresden) for helpful discussions on how to model this material.

Disclosures

The authors declare no conflicts of interest.

See Supplement 1 for supporting content.

References

1. J. Hiller, J. D. Mendelsohn, and M. F. Rubner, "Reversibly erasable nanoporous anti-reflection coatings from polyelectrolyte multilayers," Nat. materials **1**, 59–63 (2002).
2. Y.-C. Chao, C.-Y. Chen, C.-A. Lin, and J.-H. He, "Light scattering by nanostructured anti-reflection coatings," Energy & Environ. Sci. **4**, 3436–3441 (2011).
3. D. J. Aiken, "High performance anti-reflection coatings for broadband multi-junction solar cells," Sol. energy materials solar cells **64**, 393–404 (2000).
4. J. Lekner, "Omnidirectional reflection by multilayer dielectric mirrors," J. Opt. A: Pure Appl. Opt. **2**, 349 (2000).
5. M. Kolle, B. Zheng, N. Gibbons, J. J. Baumberg, and U. Steiner, "Stretch-tuneable dielectric mirrors and optical microcavities," Opt. express **18**, 4356–4364 (2010).
6. A. Saliminia, A. Villeneuve, T. V. Galstyan, S. LaRochelle, and K. Richardson, "First-and second-order bragg gratings in single-mode planar waveguides of chalcogenide glasses," J. lightwave technology **17**, 837–842 (1999).
7. N. V. Golovastikov, D. A. Bykov, L. L. Doskolovich, and E. A. Bezus, "Spatial optical integrator based on phase-shifted bragg gratings," Opt. Commun. **338**, 457–460 (2015).
8. A. V. Zayats, I. I. Smolyaninov, and A. A. Maradudin, "Nano-optics of surface plasmon polaritons," Phys. Rep. **408**, 131–314 (2005).
9. H. Tompkins and E. A. Irene, *Handbook of ellipsometry* (William Andrew Pub. Springer, Norwich, NY Heidelberg, Germany, 2005).
10. M. Warenghem, J.-F. Henninot, J.-f. Blach, O. Buchnev, M. Kaczmarek, and M. Stchakovsky, "Combined ellipsometry and refractometry technique for characterisation of liquid crystal based nanocomposites," The Rev. scientific instruments **83**, 035103 (2012).
11. D. A. Holmes and D. L. Feucht, "Electromagnetic wave propagation in birefringent multilayers," J. Opt. Soc. Am. **56**, 1763 (1966).
12. J. Schesser and G. Eichmann, "Propagation of plane waves in biaxially anisotropic layered media," J. Opt. Soc. Am. **62**, 786 (1972).
13. D. W. Berreman, "Optics in stratified and anisotropic media: 4×4–matrix formulation," J. Opt. Soc. Am. **62**, 502–510 (1972).
14. P. Yeh, "Electromagnetic propagation in birefringent layered media," J. Opt. Soc. Am. **69**, 742–756 (1979).

15. I. Hodgkinson, S. Kassam, and Q. Wu, "Eigenequations and compact algorithms for bulk and layered anisotropic optical media: Reflection and refraction at a crystal-crystal interface," J. Comput. Phys. **133**, 75–83 (1997).
16. S. J. Orfanidis, "Electromagnetic Waves and Antennas," (2016). Available online from the author.
17. M. Born and E. Wolf, *Principles of Optics* (Cambridge Univ. Press, Cambridge, England, 1997), 6th ed.
18. J. Lekner and M. C. Dorf, "Matrix methods for the calculation of reflection amplitudes," J. Opt. Soc. Am. A **4**, 2092 (1987).
19. D. Y. K. Ko and J. Inkson, "Matrix method for tunneling in heterostructures: Resonant tunneling in multilayer systems," Phys. Rev. B **38**, 9945 (1988).
20. D. Y. K. Ko and J. R. Sambles, "Scattering matrix method for propagation of radiation in stratified media: attenuated total reflection studies of liquid crystals," J. Opt. Soc. Am. A **5**, 1863–1866 (1988).
21. H. Bremmer, "The w.k.b. approximation as the first term of a geometric-optical series," Comm. Pure Appl. Math. **4**, 105–115 (1951).
22. K. Iizuka, *Elements of Photonics, Volume I: In Free Space and Special Media*, vol. 41 (John Wiley & Sons, 2002).
23. L. Li, "Bremmer series, R-matrix propagation algorithm, and numerical modeling of diffraction gratings," J. Opt. Soc. Am. A **11**, 2829 (1994).
24. J. R. Gill, E. Perivolari, M. Kaczmarek, and G. D'Alessandro, "Matlab implementation of the iterated ray method algorithm," (2021), https://doi.org/10.5258/SOTON/D1779.
25. L. Li, "Formulation and comparison of two recursive matrix algorithms for modeling layered diffraction gratings," J. Opt. Soc. Am. A **13**, 1024 (1996).
26. L. Li, "Note on the s-matrix propagation algorithm," J. Opt. Soc. Am. A **20**, 655 (2003).
27. J. Griffiths, "Ii. photochemistry of azobenzene and its derivatives," Chem. Soc. Rev. **1**, 481–493 (1972).
28. A. Priimagi and A. Shevchenko, "Azopolymer-based micro-and nanopatterning for photonic applications," J. Polym. Sci. Part B: Polym. Phys. **52**, 163–182 (2014).
29. F. P. Nicoletta, D. Cupelli, P. Formoso, G. De Filpo, V. Colella, and A. Gugliuzza, "Light responsive polymer membranes: A review," Membranes **2**, 134–197 (2012).
30. E. Mavrona, S. Mailis, N. Podoliak, G. D'Alessandro, N. Tabiryan, M. Trapatseli, J.-F. Blach, M. Kaczmarek, and V. Apostolopoulos, "Intrinsic and photo-induced properties of high refractive index azobenzene based thin films," Opt. Mater. Express **8**, 420–430 (2018).
31. E. Perivolari, J. Gill, N. Podoliak, V. Apostolopoulos, T. Sluckin, G. D'Alessandro, and M. Kaczmarek, "Optically controlled bistable waveplates," J. Mol. Liq. **267**, 484–489 (2018).
32. G. S. Kumar and D. Neckers, "Photochemistry of azobenzene-containing polymers," Chem. Rev. **89**, 1915–1925 (1989).
33. M. L. Dumont, S. Hosotte, G. Froc, and Z. Sekkat, "Orientational manipulation of chromophores through photoisomerization," in *Photopolymers and Applications in Holography, Optical Data Storage, Optical Sensors, and Interconnects,* vol. 2042 (International Society for Optics and Photonics, 1994), pp. 2–13.
34. S. Hosotte and M. Dumont, "Orientational relaxation of photomerocyanine molecules in polymeric films," Synth. metals **81**, 125–127 (1996).
35. L. De Sio, G. Klein, S. Serak, N. Tabiryan, A. Cunningham, C. M. Tone, F. Ciuchi, T. Bürgi, C. Umeton, and T. Bunning, "All-optical control of localized plasmonic resonance realized by photoalignment of liquid crystals," J. Mater. Chem. C **1**, 7483–7487 (2013).
36. S. Nersisyan, N. Tabiryan, D. M. Steeves, and B. R. Kimball, "Axial polarizers based on dichroic liquid crystals," J. Appl. Phys. **108**, 033101 (2010).
37. G. Pawlik, A. C. Mitus, J. Mysliwiec, A. Miniewicz, and J. G. Grote, "Photochromic dye semi-intercalation into dna-based polymeric matrix: Computer modeling and experiment," Chem. Phys. Lett. **484**, 321–323 (2010).
38. F. You, M. Y. Paik, M. Häckel, L. Kador, D. Kropp, H.-W. Schmidt, and C. K. Ober, "Control and suppression of surface relief gratings in liquid-crystalline perfluoroalkyl–azobenzene polymers," Adv. Funct. Mater. **16**, 1577–1581 (2006).
39. O. Yaroshchuk and Y. Reznikov, "Photoalignment of liquid crystals: basics and current trends," J. Mater. Chem. **22**, 286–300 (2012).
40. Q. Guo, A. K. Srivastava, V. G. Chigrinov, and H. S. Kwok, "Polymer and azo-dye composite: a photo-alignment layer for liquid crystals," Liq. crystals **41**, 1465–1472 (2014).
41. L. Miccio, M. Paturzo, A. Finizio, and P. Ferraro, "Light induced patterning of poly (dimethylsiloxane) microstructures," Opt. express **18**, 10947–10955 (2010).
42. N. Tsutsumi, "Recent advances in photorefractive and photoactive polymers for holographic applications," Polym. Int. **66**, 167–174 (2017).
43. R. J. Moerland and J. P. Hoogenboom, "Subnanometer-accuracy optical distance ruler based on fluorescence quenching by transparent conductors," Optica **3**, 112–117 (2016).
44. T. A. Konig, P. A. Ledin, J. Kerszulis, M. A. Mahmoud, M. A. El-Sayed, J. R. Reynolds, and V. V. Tsukruk, "Electrically tunable plasmonic behavior of nanocube–polymer nanomaterials induced by a redox-active electrochromic polymer," ACS nano **8**, 6182–6192 (2014).